Metabotropic action of postsynaptic kainate receptors triggers hippocampal LTP

Milos M. Petrovic[1,3,4,5*], Silvia Viana da Silva[2], James P. Clement[6], Ladislav Vyklicky[4], Christophe Mulle[2], Inmaculada M González-González[1†*], and Jeremy M. Henley[1†*]

[1]School of Biochemistry, University of Bristol, Bristol, UK

[2]Interdisciplinary Institute for Neuroscience, University of Bordeaux, Bordeaux, France.

[3]School of Pharmacy and Biomedical Sciences, University of Central Lancashire, Preston, UK (present address)

[4]Institute of Physiology, Academy of Sciences, Prague, Czech Republic

[5]Insitute of Medical Physiology, School of Medicine, University of Belgrade, Serbia

[6]Neuroscience Unit, Jawaharlal Nehru centre for Advanced Scientific Research, Bangalore, India

[*] Co-corresponding authors

[†] Joint last authors

Please address correspondence to: JMH (J.M.Henley@bristol.ac.uk), IMG-G (ggonzalezmi@gmail.com) or MMP (mpetrovic@uclan.ac.uk)

Abstract

Long-term potentiation (LTP) in the rat hippocampus is the most extensively studied cellular model for learning and memory. Induction of classical LTP involves an NMDA receptor- and calcium-dependent increase in functional synaptic AMPA receptors mediated by enhanced recycling of internalized AMPA receptors back to the postsynaptic membrane. Here we report a novel, physiologically relevant NMDA receptor-independent mechanism that drives increased AMPA receptor recycling and LTP. This pathway requires the metabotropic action of kainate receptors and activation of G-protein, protein kinase C and phospholipase C. Like classical LTP, kainate receptor-dependent LTP recruits recycling endosomes to spines, enhances synaptic recycling of AMPA receptors to increase their surface expression and elicits structural changes in spines, including increased growth and maturation. These data reveal a new and previously unsuspected role for postsynaptic kainate receptors in the induction of functional and structural plasticity in the hippocampus.

Introduction

The precise dynamic regulation of the number, composition and distribution of postsynaptic AMPA receptors (AMPARs) is essential for synaptic transmission and plasticity. Classical LTP, which has been characterised extensively in many brain areas, requires the activation of NMDA receptors (NMDARs) [1]. An equivalent NMDAR-dependent LTP can be induced in cultured hippocampal neurons by brief exposure to the NMDAR co-agonist glycine, which elicits the insertion of AMPARs into the postsynaptic membrane and increases miniature excitatory postsynaptic currents (mEPSCs) [2].

LTP involves both recycling-dependent increases in AMPAR surface expression at the post-synaptic membrane and increases in dendritic spine size [3]. Furthermore, stimuli that induce LTP in dispersed hippocampal neuronal cultures promote recycling and recruitment of transferrin receptor-positive recycling endosomes into spines. This repositioning of the endosomal-recycling compartment is critical for activity-dependent changes in spine morphology and provides a mechanistic link between structural and functional plasticity [3, 4].

Kainate receptors (KARs) are tetrameric assemblies of combinations of GluK1 – GluK5 subunits. They are present at both pre- and postsynaptic membranes where they perform distinct roles in modulating synaptic transmission, neuronal excitability and network activity [5, 6], and are implicated in processes ranging from neuronal development and differentiation to neurodegeneration and neuronal cell death [5, 7]. In addition to direct ionotropic signalling, KARs also signal through the activation of G proteins leading to PKC activation [5, 6, 8-10]. Under physiological glutamate release conditions, postsynaptic KAR metabotropic signalling in CA1 and CA3 pyramidal neurones inhibits the hyperpolarisation caused by the post-spike potassium current I (sAHP) [11-14].

We, and others, have shown previously that transient kainate (KA) stimulation modulates surface expression of KARs [15-18] via changes in Rab11-dependent recycling within spines [19]. Here, we report that KA induces an NMDAR-independent increase in the synaptic surface expression of functional AMPARs, as well as the structural plasticity via a pathway that requires metabotropic signalling of postsynaptic GluK2-containing KARs and enhanced endosomal vesicle recycling in spines.

Results

KAR activation increases surface expression of functional synaptic AMPARs.

We first investigated the effects of KA application on AMPAR surface expression in the presence of tetrodotoxin (TTX, 0.5 µM), GYKI53655 (40 µM) and L689560 (5 µM) to suppress activity-dependent glutamate release and prevent activation of AMPARs and NMDARs respectively. Agonist stimulation of KARs (10 µM KA, 3 min) significantly increased surface expression of both GluA1 and GluA2 AMPAR subunits (Fig. 1A, $p=0.001$ and $p=0.004$, respectively), without altering the total number of AMPARs (Supplementary Fig.1A-B, $p>0.09$). This KAR-induced increase in plasma membrane expressed AMPARs was blocked by the competitive AMPAR/KAR antagonist CNQX (10 µM; Fig. 1A, $p>0.9$).

To define if the KAR-induced increase in AMPAR surface expression occurred at spines, we immuno-labelled surface expressed GluA1 and GluA2 in non-permeabilised neurons (Fig. 1B) and calculated the spine/adjacent dendrite ratio. This was increased for both GluA1 and GluA2 following KAR stimulation ($p=0.001$ for GluA1 and $p=0.003$ for GluA2), indicating preferential AMPAR surface expression in spines. Consistent with this, KAR-stimulation increased surface GluA1 and GluA2 colocalisation with the postsynaptic marker PSD95 (Fig. 1C, $p<0.001$).

The increase in synaptic GluA1 and GluA2 was induced by a brief (3 min) exposure of the cultured hippocampal neurons to all KA concentrations tested, ranging from 500 nM to 20 µM (Supplementary Fig. 1C-D, $p<0.001$ and $p<0.001$ respectively). We next tested if nanomolar concentrations of KA increased postsynaptic AMPAR-mediated mEPSCs in CA1 pyramidal neurons in hippocampal slices. KA concentrations below 3 µM do not activate AMPARs in CA1 [20], but, to fully exclude direct KA activation of AMPARs, we co-applied the AMPAR specific antagonist GYKI53655 (40 µM) during the transient KA application. GYKI53655 was then washed out to obtain AMPAR mEPSCs. Co-application of GYKI53655 with 500 nM KA did not change mEPSC frequency (Supplementary Fig. 2A, $p>0.3$) but caused a marked increase in the amplitude of mEPSCs (Fig. 1D and Supplementary Fig. 3A, $p<0.004$. These data demonstrate a KAR-induced increase of functional postsynaptic AMPARs.

KAR-mediated NMDAR-independent LTP.

Increased postsynaptic AMPARs surface expression underpins LTP, so we investigated the effects of KAR activation on synaptically evoked AMPAR-mediated excitatory postsynaptic responses in rat hippocampal slices. KA (10 µM, 3 min) caused a transient depression followed by a progressive increase in AMPAR-mediated CA1 EPSCs (Supplementary Fig. 4A; 169.8% ± 31.4%, p=0.01) with no change in glutamate release probability determined by the paired-pulse ratio (PPR; Supplementary Fig. 4B) in the continuous presence of 100 µM APV (to block NMDARs). At this concentration, however, KA activates AMPARs and could affect their dynamics. Thus, we performed the experiment as above, but using 40 µM GYKI53655 (present prior to and during KA application to block AMPARs). Although in the presence of GYKI53655 there was a significant difference in amplitude between the control and KA conditions (KA, 100.8% ± 15.5%; Control 54.6% ± 8.0%, p=0.009; Supplementary Fig. 4C, unchanged PPRs are shown in Supplementary Fig. 4D and representative responses shown in Supplementary Fig. 4E), GYKI53655 masked the time course of AMPAR-mediated EPSCs. We therefore reduced the KA concentration to 500 nM, thereby avoiding the need to block AMPARs with GYKI53655. Under these conditions, 500 nM KA caused a progressive and persistent increase in AMPAR-mediated CA1 EPSCs (Figure 2A; 133.1% ± 11.4%, p=0.02), reaching a peak approximately 10-15 min after the agonist application. Again, we found no change in PPR (Supplementary Fig. 4F, p>0.3). Combined with our mEPSC data, these evoked EPSC results indicate that KAR activation elicits NMDAR-independent KA-induced LTP via increased surface expression of postsynaptic AMPARs in CA1 hippocampal neurons.

Consistent with this, KA did not induce any potentiation in AMPAR-mediated field potentials in the CA1 region of hippocampal slices from GluK2-knockout ($GluK2^{-/-}$) mice (95.7 ± 3.6 %, p > 0.05, Supplementary Fig 5A). To exclude any possible developmental effects in the GluK2-knockout mice, we tested the effect of acutely blocking KARs in wild-type mice using the AMPAR/KAR blocker CNQX (10 µM) prior to and during KA challenge, followed by CNQX washout (Supplementary Fig. 5B). Compared to sham controls (CNQX only), the recovery profile was unchanged (80.2 ± 3.4 % vs. 78.7 ± 9.5 % for KA and control, p > 0.05). We also confirmed that KA application potentiated AMPAR responses in hippocampal slices obtained from adult, 3-month old mice (124.7 ± 9.6%, p < 0.01) (Supplementary Fig. 5C-D), indicating that KA-induced LTP is not developmentally restricted.

Using wild-type and GluK2-knockout mice, we next examined the KAR dependency of a previously reported NMDAR-independent form of LTP evoked by high frequency stimulation (HFS) protocol, based on the modified procedure from [21, 22] (illustrated in schematic form in Fig. 2B and described in Methods). As shown in Supplementary Fig. 6A-C, field potential recordings revealed robust LTP in acute hippocampal slices from wild-type mice (185.8 ±

26.1% vs.106.1 ± 5.2% in test vs. control pathway, p=0.007), whereas a reduced LTP was obtained in GluK2-knockout mice (170.3 ± 17.3% vs.106.2 ± 5.7% in test vs. control pathway, p=0.03). To isolate the NMDAR-independent component of this LTP, we used 50 µM D-APV, which completely blocked LTP in the GluK2-knockout (106.3 ± 5.0% vs. 99.4 ± 4.6% in test vs. control pathway, p>0.5), but not in WT mice (128.5 ± 11.4% vs.107.7 ± 5.0% in test vs. control pathway, p<0.02). No changes in PPR were observed (Supplementary Fig. 6D). These data confirm that activation of GluK2-containing KARs by synaptically released glutamate induces NMDAR-independent and KAR-dependent hippocampal LTP.

Consistent with previous reports [22], the NMDAR-independent component of this HFS LTP in wild-type mice was blocked by the L-type calcium blocker nifedipine (110.45 ± 3.66% vs. 104.05 ± 3.81%, p>0.05, test vs. control pathway, Supplementary Fig. 7A). As in previous experiments, no change in the PPR was detected (Supplementary Fig. 7B).

Although widely used, HFS does not correspond to intrinsic *in vivo* patterns of hippocampal activity. Therefore, to determine if KAR-dependent LTP can be induced by more physiological stimuli, we used a protocol based on hippocampal sharp-wave/ripple-like stimulation pattern (RL-LTP; illustrated in schematic form in Fig. 2C) [23]. In wild-type mice, the RL-LTP protocol resulted in a progressive potentiation that peaked 10-15 min after stimulation (Fig. 2D left panel; 166.2 ± 8.5 % vs 101.1 ± 2.9% in test vs control pathway, p<0.001). In GluK2-knockout mice (Fig. 2D right panel; representative traces in Fig. 2E), there was a significantly reduced LTP (139.7 ± 7.5 % vs.100.6 ± 2.7% in test vs. control pathway, p<0.001, and p=0.03 compared to wild-type mice, Fig. 2F). Importantly, however, while RL-LTP (although at reduced level) was still detected in wild-type mice in the presence of 50 µM D-APV (Fig 2D left panel; 120.9 ± 2.3% vs 99.5 ± 2.8% in test vs control pathway, p<0.001), RL-LTP was completely prevented in GluK2-knockout mice (99.1 ± 4.0% vs 99.2 ± 3.8%, test vs control pathway, p=0.98, and p=0.002 compared to wild-type mice).

D-APV is a competitive antagonist, therefore, to exclude the theoretical possibility that the intense RL-LTP stimulation paradigm could lead to glutamate accumulation in synaptic cleft that could out-compete D-APV, thereby allowing NMDAR-dependent LTP, we used a previously described strategy [24]. We first blocked the NMDARs with MK-801 (20 µM), a use-dependent blocker (in nominal 0 mM Mg^{2+} aCSF, to facilitate the NMDAR activation). Then, once the full blockade was achieved, we reintroduced ordinary aCSF, continuously supplemented with MK-801 (20 µM) and D-AP5 (50 µM). Robust potentiation still occurred in wild-type mice, further confirming the KAR-dependent component of RL-LTP (142.6 ± 0.6 *vs.* 98.2 ± 9.3% in test *vs.* control pathway, p<0.01; Supplementary Fig. 7C-D).

Finally, to further discount any possible confounding developmental issues in GluK2-knockout mice, we performed the RL-LTP experiment in wild-type mice while acutely blocking KARs using CNQX (10 µM, present prior to and during LTP induction, followed by washout), similarly to the approach used in Supplementary Fig. 5B. No RL-LTP was induced after full inhibition by CNQX, *i.e.* both test and control pathways gradually recovered with similar temporal profiles (Supplementary Fig. 7E, minutes 37-41: 20.9 ± 4.6 % vs. 22.3 ± 3.2, $p > 0.05$; minutes 57-61: 75.1 ± 6.00 % vs. 70.9 ± 6.46 %, $p > 0.05$; minutes 77-81: 100.4 ± 0.7 % vs. 100.5 ± 2.6 %, $p > 0.05$, test *vs.* control pathway). These results provide compelling evidence that physiologically relevant stimulation of GluK2-containing KARs can induce NMDAR-independent LTP in the hippocampus.

Next, using rat hippocampal slices, we performed within-slice comparisons of test and control pathway responses to RL-LTP and KA application. First we induced RL-LTP (normalized fEPSP slope in test and control pathway = 123.1 ± 1.8% and 98.1 ± 1.6%, respectively, $p<0.001$, Supplementary Fig. 8A-C). We then subjected the slice to bath application of KA (500 nM, 3 min), which caused a robust increase in control pathway to levels equivalent to the RL-LTP in the test pathway (normalized fEPSP slope in test and control pathway = 132.9 ± 2.4% and 131.7 ± 3.6%, respectively; $p=0.78$). Importantly, however, there was no further increase in the pathway previously subjected to RL-LTP. These data also demonstrate that the extent of agonist-induced LTP in field recordings is comparable to that achieved by patch-clamp recording.

Our data from GluK2$^{-/-}$ mice indicate that LTP is not saturated in the presence of D-APV because RL-LTP induced significantly stronger LTP in WT mice. In a complementary approach, we directly tested if agonist and electrical stimulation-induced KAR-LTP share a common mechanism using a previously established occlusion protocol [25] .

We initially induced RL-LTP in one pathway (black circles, Supplementary Fig. 8D, 100.9 ± 2.05 % vs. 133.4 ± 10.00%, $p<0.05$) and then bath applied KA (500 nM, 3 min). As expected, and consistent with the data in Supplementary Fig. 8A, the pathway that had not been subjected to RL-LTP was potentiated by kainate (white circles, Supplementary Fig. 8D-E, 118.1 ± 4.0 %, $p < 0.01$). Importantly, KA did not cause additional potentiation in the pathway previously exposed to RL-LTP (black circles, 128.0 ± 11.2 %, $p > 0.05$). The stimulation intensity of the *test* pathway (white circles) was then adjusted to normalise it to its basal level (101.6 ± 5.7 %, $p > 0.05$) and the RL-LTP protocol was then delivered to this pathway (Supplementary Fig. 8D-E). Since no further potentiation was observed (97.6 ± 9.3 %, $p > 0.05$), this inverse occlusion experiment confirms that KA-induced potentiation and RL-LTP share a common mechanism.

KAR activation induces structural plasticity via enhanced endosomal recycling.

NMDAR-dependent LTP elicits structural changes in spine shape and increased spine size [4]. Correspondingly, transient KA application robustly increases spine density and maturity (Fig. 3A-C), More specifically, there are increases in mature spine size (65.1% ± 14%, p<0.001; Fig. 3A) and numbers of dendritic protrusions (68.9% ± 25%, p<0.001; Fig. 3B), as well as enhanced transition from stubby to mushroom spines (18.7% ± 4%, p<0.001; Fig. 3C).

NMDAR-dependent LTP also enhances generalised endosomal recycling of cargo proteins and membrane within the spine [3, 4]. To investigate if the same mechanisms underlie KAR-dependent LTP, we monitored transferrin-Alexa594 (Tf-A594) labelled recycling endosomes. Tf-A594 endosomes distribute mainly at the base of spines in non-stimulated control neurons. Following transient KA application, however, Tf-A594 endosomes translocate from the dendritic shaft to the spine head (Fig. 4A). Furthermore, expression of a dominant negative version of the recycling endosome-associated small GTPase Rab11 (Rab11dn), which blocks NMDAR-dependent LTP [26], prevented the KAR-evoked recruitment of recycling endosomes into spines (Fig. 4B) and blocked the increases in the head diameter of mushrooms spines (p<0.0001 for KA - control, and Rab11wt - Rab11dn; Fig. 4C).

To confirm the role of recycling in KAR-dependent LTP, we used surface biotinylation assays in combination with primaquine to selectively inhibit recycling [27] or monensin to block both recycling and lysosomal degradation [28]. As expected, both drugs prevented the KAR-induced increase in GluA1 and GluA2 surface expression (Supplementary Fig. 9A-B, p<0.001). We next quantified surface expression of GluA1 and GluA2 in spines and adjacent shaft regions. Inhibiting recycling with primaquine, monensine or Rab11dn prevented the KAR-induced change in the spine:dendrite ratio of AMPAR surface expression (Supplementary Fig. 10A-C, p=0.18 for GluA1 and p=0.24 for GluA2, p=0.80 GluA1 and p=0.34 GluA2, and p=0.03 for GluA1 and p=0.02 for GluA2). These data indicate that both NMDAR- and KAR-dependent LTP require the recruitment and enhanced recycling of endosomal vesicles in spines.

KAR-dependent LTP is mediated via a non-canonical G-protein-associated signalling pathway.

Although some mechanistic details are still lacking, it is now clear that KARs signal via G-protein-dependent pathways to increase intracellular calcium $[Ca^{2+}]_i$, and activate protein kinase C (PKC) and phospholipase C (PLC) [5, 6, 9, 10, 29]. Since increased $[Ca^{2+}]_i$ is required for LTP, [30, 31] we tested the source of $[Ca^{2+}]_i$ increase in KAR-dependent LTP using the extracellular chelator EDTA and the membrane permeant chelator BAPTA-AM. The presence of BAPTA-AM, but not EDTA, during the KA application blocked the KAR-evoked increase in synaptic AMPAR surface expression (Fig. 5A, B; controls without KA shown in

Supplementary Fig. 11A; BAPTA-AM; GluA1, p=0.5; GluA2 p= 0.10: EDTA; GluA1 p=0.009; GluA2 p<0.001) and the associated changes in the structural plasticity (Fig. 5C and Supplementary Fig. 11B, EDTA; p <0.001; BAPTA-AM p=0.61). Similarly, preincubation with PKC inhibitor chelerythrine or the PLC inhibitor U73122 blocked the KAR-induced increase in GluA1 and GluA2 expression at synapses (Fig. 5A, B; controls without KA shown in Supplementary Fig. 11A-B; U73122: GluA1 p=0.56; GluA2 p= 0.32 ; chelerythrine: GluA1 p=0.54, GluA2 p= 0.78), the increase in the spine size (Fig. 5C and Supplementary Fig. 11B, U73122: p=0.42; chelerythrine: p=0.48), as well as the agonist-evoked KAR-dependent LTP in electrophysiological recordings (100.5 ± 1.4%, p > 0.05 for U73122 and 100.7 ± 5.8%, p>0.05 for chelerythrine, Fig. 5D, E).

We also analysed PKC and PLC activity in cells after triggering KAR-dependent LTP. Brief KAR stimulation (3 min, 500nM) elicited a nearly 2-fold increase in PLC and PKC activity compared to unstimulated cells (Fig. 5F). Furthermore, the extent of PKC activation in KAR-dependent LTP is similar to stimulation by the phorbol ester PMA (0.5 µM, 3min, p=0.4). The KAR-induced activation of PKC and PLC was prevented by CNQX and BAPTA-AM, but not by the presence of EDTA during KA application (Fig. 5F: PKC: +CNQX: p=0.037, +EDTA: p=0.81, +BAPTA-AM, p=0.002, +Chelerythrine p=0.038. For PLC: +CNQX: p=0.047, +EDTA: p=0.84, +BAPTA-AM: p=0.056, +U73122 p=0.006). Finally, in addition to EGTA (5 mM) application only during KA application, we continuously applied (30 min during and after KA application) the selective Ca^{2+} chelator EGTA to bind extracellular Ca^{2+} or nifedipine to block L-type voltage-gated Ca^{2+} channels (VGCCs). Continuous application of either drug prevented the KA-induced increase in GluA1 and GluA2 surface expression at synapses (Supplementary Fig. 11C, D; p<0.001), suggesting a delayed role for extracellular Ca^{2+} in KAR-LTP. Importantly, inhibiting Group I /II metabotropic glutamate receptors with the specific antagonist MCPG did not affect KAR-dependent increases in synaptic AMPARs or spine size. (Supplementary Fig. 12A, B; p<0.001 and p=0.018). These data demonstrate that KAR-LTP requires activation of PKC and PLC and intracellular calcium release, consistent with a KAR-mediated metabotropic signalling pathway.

Furthermore, we performed the same experiments as those shown in Figure 1C, but with the preincubation in the presence of G-protein inhibitor pertussis toxin (PTX) (1 µg/mL, 1 hour). PTX prevented KA-induced activation of both PLC and PKC (Fig. 6A, p=0.03 and p=0.012 respectively). PTX also blocked the increased colocalization of GluA1 and GluA2 with PSD95 following the KA challenge (Fig. 6B, GluA1, p=0.93; GluA2 p=0.47, compare with Fig. 1C). Furthermore, incubation of hippocampal slices with PTX prior to recording mEPSCs prevented the KAR-induced increase in AMPAR mEPSC amplitude in CA1 pyramidal neurons (Fig. 6C, p=0.34, compare with Fig. 1D), with no change in the frequency

(Supplementary Fig. 13A p>0.1). Correspondingly, agonist-evoked and electrically stimulated KAR-dependent LTP (Fig. 6D-E and Supplementary Fig. 13B-D, p=0.69 and p=0.3, compare with Fig. 2A), as well as structural plasticity (Fig. 6F and Supplementary Fig. 13E, p=0.4, compare with Fig. 3A) were prevented by preincubation with PTX, again indicating the requirement for a metabotropic action for KARs.

Both our imaging and functional data using nifedipine suggest that following initial LTP induction that requires intracellular Ca^{2+}, extracellular calcium entry through L-type VGCCs plays a role in maintaining KAR-LTP. Moreover, VGCC currents can be modulated by G-protein activation [32]. We therefore used patch-clamp electrophysiology to measure VGCC Ca^{2+} currents. KA application (500 nM, 3 min) increased VGCC currents in control conditions (127.4 ± 16.1%, n = 5), but there was no increase in slices that had been preincubated with PTX (90.4 ± 4.5%, n = 4, $p < 0.05$, Supplementary Fig. 14).

Substitution of extracellular Na^+ with an equimolar concentration of the non-permeant cation N-methyl-D-glucamine (NMDG) prevents KAR channel conductance, but does not impede metabotropic KAR activity [9]. Replacing Na^+ with NMDG does not block the KAR-induced increase in GluA1 and GluA2 colocalization with PSD95 and spine size (Supplementary Fig.15A-B; GluA1, p= 0.004, GluA2, p <0.001and p=0.009 for spine size), further confirming that ionotropic activity is not required for KAR-dependent LTP. The KAR antagonist UBP310 has been reported to inhibit KAR ionotropic activity, but not KAR-metabotropic signalling, via a mechanism that likely involves an action beyond simple competitive antagonism [33]. This effect is unlikely to be due to different subunit compositions since most KARs in the brain comprise GluK2/5 combinations. We anticipate that future studies will uncover the mechanisms underlying this selective inhibition of ionotropic over metabotropic KAR activity. Nonetheless, consistent with the documented selectively ionotropic action,UBP310 (10 μM) did not block KA-induced increases in PLC and PKC activity (Fig. 7A, p= 0.74 and p=0.94 compared to KA) nor did it prevent KAR-dependent LTP (Fig. 7B-C and Supplementary Fig.15C-D p=0.01 and p=0.006) and structural spine plasticity (Fig.7D, p=0.03)).

Taken together, this array of complementary and mutually supportive data provide compelling evidence that KAR channel activity is not required for KAR-dependent LTP, but is instead underpinned by KAR-mediated metabotropic signalling.

Discussion

Here we report that KAR activation can elicit a previously unanticipated form of NMDAR-independent LTP. This occurs via a metabotropic KAR pathway that recruits endosomal recycling machinery from the dendritic shaft into the spine to alter post-endocytic GluA1 and GluA2 sorting and exocytosis back to the spine plasma membrane.

KAR activation increases AMPAR surface expression at postsynapse

We have shown previously that transient KA application can increase KAR surface expression [16] and enhance spine growth by altering post-endocytic sorting and enhanced recycling mechanisms [19]. Furthermore, KARs regulate neurite outgrowth [16, 34, 35], as well as filopodia and nascent spinule development [36]. Here we show that transient KAR activation augments recycling and surface expression of AMPARs, increases AMPAR colocalisation with PSD95 in spines and increases the amplitude of AMPAR mEPSCs. Consistent with postsynaptic mechanisms, the probability of neurotransmitter release was unchanged. Furthermore, using two different stimulation protocols, we demonstrate that synaptic activation of GluK2-containing KARs underlies the increases in the evoked AMPAR-mediated responses. These results reveal a novel and physiologically relevant form of postsynaptic KAR-dependent, NMDAR-independent LTP.

KAR activation increases synaptic recycling and spine size

In parallel with increased AMPAR-mediated neurotransmission, NMDAR-dependent LTP elicits the formation and enlargement of dendritic spines to consolidate neural circuitry [37, 38]. Recycling endosomes are recruited to deliver membrane material directly within spines for structural plasticity [3, 4], providing a mechanistic link for coupling changes in spine size to the regulation of AMPAR-mediated transmission and LTP [39]. Like NMDAR-dependent LTP, KAR-dependent LTP requires translocation of Rab11-positive recycling endosomes from the dendritic shaft into spines. Moreover, overexpression of dominant negative Rab11, which blocks NMDAR-dependent LTP [40], prevents the KAR-evoked redistribution of recycling endosomes to spines and blocks KAR-dependent LTP. This involvement of Rab11 in NMDAR-dependent and KAR-dependent LTP indicates shared mechanisms in both pathways.

Metabotropic actions of KARs mediate KAR-dependent LTP

Metabotropic KAR signalling was first identified through the KAR-mediated modulation of GABA release, which does not require KAR channel activation, but is prevented by inhibition of G-protein and PKC activity [8]. Subsequently, KAR-dependent inhibition of the slow after-hyperpolarizing potential (sAHP), which enhances neuronal excitability, was also shown to be mediated by metabotropic KAR signalling [11]. Although there is now a wealth of experimental support for metabotropic action of both pre- and postsynaptic KARs (for reviews see [5, 6, 41]), many questions remain. For example, the identity of the KAR subunit conferring metabotropic action is unclear because the literature is contradictory and no KAR subunits contain conventional G-protein binding motifs. Nonetheless, it is now generally accepted that metabotropic KAR signalling is PTX sensitive and thus involves Go rather than

Gq protein activation. Accordingly, a recent report has suggested that the KAR subunit GluK1 can associate directly with a Go protein α subunit and that this association is responsible for the metabotropic effects of KARs [10]. Our results now reveal an entirely novel role for metabotropic KAR signalling in regulating AMPAR trafficking, spine morphology and NMDAR-independent LTP.

KAR-dependent LTP

LTP at CA1 hippocampal synapses is not uniform and comprises a range of NMDAR-dependent and -independent plasticity mechanisms [42]. Given the crucial importance of plastic changes in the brain, this array of pathways provides a dynamic, flexible and reliable system to ensure the continuity of neuronal network and brain function. Our identification of a novel postsynaptic KAR-dependent LTP adds to these important system traits. Ripple-like high-frequency patterns of activity (~200 Hz for ~100 ms, repeating at ~1 Hz) occur in immobile awake animals and during slow wave sleep [43]. These patterns generally occur in conjunction with large-amplitude sharp waves and ripple-related activity *in vivo* is implicated in LTP that underlies memory consolidation in the hippocampus [44, 45]. Here, we show for the first time that this strong and physiologically relevant ripple-like activity LTP induction protocol (RL-LTP) is mediated via GluK2-containing KARs.

It is notable that the induction of KAR-LTP and the previously reported agonist-evoked increase in surface expression of GluK2-containing KARs share a similar time course that reaches a plateau 10-15 min after stimulation [16]. This profile correlates with the delayed NMDAR-independent component of HFS-induced LTP [21] and shares dependency on VGCC activation. Moreover, G-protein potentiation of VGCC activity is sensitive to PTX and requires PKC activation and increases in $[Ca^{2+}]_i$ [32], consistent with KAR-metabotropic actions modulating VGCC activity in NMDAR-independent LTP. These features are similar to the role of mGluR5 receptor metabotropic signalling which, by facilitating L-type VGCC activity via intracellular Ca^{2+} release, contributes to NMDAR-independent forms of LTP [46]. It is important to note that the rise in $[Ca^{2+}]_i$, presumably mediated via IP3 receptors, can facilitate VGCC activity and that VGCC activity and the influx of extracellular calcium can prolong the temporal profile and frequency of intracellular Ca^{2+}-release events [47]. This reciprocal feedback system fits with our imaging and electrophysiological experiments with nifedipine and can extend beyond the kainate stimulation. We anticipate that future work will explore this feedback system in more detail by combining simultaneous multiphoton imaging and electrophysiology in brain slices.

Concluding remarks

Here we describe an entirely new pathway in which direct activation of postsynaptic KARs induces LTP. These data show that KAR metabotropic signalling facilitates information transfer and synaptic integration by two parallel mechanisms, namely the short-term regulation of excitability [13, 14] and long term increase in synaptic efficacy via LTP. Both mechanisms are induced by high frequency stimulation of KARs and require PKC. Given that KARs are highly expressed during the neuronal circuit formation, and that their dysfunction is implicated in many neurological diseases including epilepsy [48] and intellectual disability [49], we anticipate that our findings will have far reaching implications.

Acknowledgements

We are grateful for financial support from the ERC (Proposal n° 232881), MRC (MR/L003791), BHF (PG/14/60/31014) and BBSRC (BB/K014366 and BB/K014358) to JMH; EMBO Fellowships to MIGG (ALTF 224-2009 and ASTF 438-2011) and MMP (ASTF 232-2011); MRC (MR/M023729/1) to MMP; the Centre National de la Recherche Scientifique, the Conseil Régional d'Aquitaine, the Labex BRAIN and the Fundacao para a Ciencia e a Tecnologia to CM and SVS; the Czech Science Foundation (GACR): 17-02300S; P304/12/G069) and Research Project of the AS CR RVO (67985823) to LV; the Department of Science and Technology (DST) – Young Scientist Scheme (SERB/LS-779/2013) to JPC. We are grateful to P. Rubin and N. Grosjean for excellent technical support, A. Singh for his help in some follow-up experiments and to J. Esteban (CBMSO, Madrid) for providing Rab constructs.

Author contributions

MIGG designed and performed the biochemistry and imaging experiments and participated in electrophysiological experiments; MMP designed and performed agonist and stimulation evoked electrophysiology and participated in imaging experiments. SVS did electrophysiology in wild-type and GluK2$^{-/-}$ mice hippocampal slices; CM provided knockout mice and extensive advice; JPC performed the MK-801/D-APV and CNQX dual pathway electrophysiological experiments. LV provided facilities and reagents and helped analyse the electrophysiological data. JMH instigated the study and provided overall supervision and management. JMH, MIGG and MMP designed the study, analysed the data and wrote the paper. All authors discussed the results and commented on the manuscript.

Author Information

The authors declare no competing financial interests.

References

1. Malenka, R.C. & Bear, M.F. LTP and LTD: an embarrassment of riches. *Neuron* **44**, 5-21 (2004).
2. Lu, W.*, et al.* Activation of synaptic NMDA receptors induces membrane insertion of new AMPA receptors and LTP in cultured hippocampal neurons. *Neuron* **29**, 243-254. (2001).
3. Park, M., Penick, E.C., Edwards, J.G., Kauer, J.A. & Ehlers, M.D. Recycling endosomes supply AMPA receptors for LTP. *Science* **305**, 1972-1975 (2004).
4. Park, M.*, et al.* Plasticity-induced growth of dendritic spines by exocytic trafficking from recycling endosomes. *Neuron* **52**, 817-830 (2006).
5. Contractor, A., Mulle, C. & Swanson, G.T. Kainate receptors coming of age: milestones of two decades of research. *Trends Neurosci* **34**, 154-163 (2011).
6. Lerma, J. & Marques, J.M. Kainate receptors in health and disease. *Neuron* **80**, 292-311 (2013).
7. González-González, I.M.*, et al.* Kainate Receptor Trafficking. *WIRES Membrane Trasnsport and Signalling* **1**, 31-44 (2012).
8. Rodriguez-Moreno, A. & Lerma, J. Kainate receptor modulation of GABA release involves a metabotropic function. *Neuron* **20**, 1211-1218. (1998).
9. Rozas, J.L., Paternain, A.V. & Lerma, J. Noncanonical signaling by ionotropic kainate receptors. *Neuron* **39**, 543-553 (2003).
10. Rutkowska-Wlodarczyk, I.*, et al.* A Proteomic Analysis Reveals the Interaction of GluK1 Ionotropic Kainate Receptor Subunits with Go Proteins. *J Neurosci* **35**, 5171-5179 (2015).
11. Melyan, Z., Wheal, H.V. & Lancaster, B. Metabotropic-mediated kainate receptor regulation of IsAHP and excitability in pyramidal cells. *Neuron* **34**, 107-114 (2002).
12. Fisahn, A., Heinemann, S. & McBain, C.J. The Kainate Receptor Subunit GluR6 Mediates Metabotropic Regulation of the Slow and Medium AHP Currents in Mouse Hippocampal Neurons. *J Physiol* (2004).
13. Melyan, Z., Lancaster, B. & Wheal, H.V. Metabotropic regulation of intrinsic excitability by synaptic activation of kainate receptors. *J Neurosci* **24**, 4530-4534 (2004).
14. Ruiz, A., Sachidhanandam, S., Utvik, J.K., Coussen, F. & Mulle, C. Distinct subunits in heteromeric kainate receptors mediate ionotropic and metabotropic function at hippocampal mossy fiber synapses. *J Neurosci* **25**, 11710-11718 (2005).
15. Rivera, R., Rozas, J.L. & Lerma, J. PKC-dependent autoregulation of membrane kainate receptors. *EMBO J* **26**, 4359-4367 (2007).

16. Martin, S., Bouschet, T., Jenkins, E.L., Nishimune, A. & Henley, J.M. Bidirectional regulation of kainate receptor surface expression in hippocampal neurons. *J Biol Chem* **283**, 36435-36440 (2008).
17. Selak, S.*, et al.* A role for SNAP25 in internalization of kainate receptors and synaptic plasticity. *Neuron* **63**, 357-371 (2009).
18. Carta, M.*, et al.* CaMKII-dependent phosphorylation of GluK5 mediates plasticity of kainate receptors. *EMBO J* **32**, 496-510 (2013).
19. Gonzalez-Gonzalez, I.M. & Henley, J.M. Postsynaptic Kainate Receptor Recycling and Surface Expression Are Regulated by Metabotropic Autoreceptor Signalling. *Traffic* (2013).
20. Bureau, I., Bischoff, S., Heinemann, S.F. & Mulle, C. Kainate receptor-mediated responses in the CA1 field of wild-type and GluR6-deficient mice. *J Neurosci* **19**, 653-663 (1999).
21. Grover, L.M. & Teyler, T.J. Normal-Methyl-D-Aspartate Receptor-Independent Long-Term Potentiation in Area CA1 of Rat Hippocampus - Input-Specific Induction and Preclusion in a Non-Tetanized Pathway. *Neuroscience* **49**, 7-11 (1992).
22. Grover, L.M. & Teyler, T.J. Two components of long-term potentiation induced by different patterns of afferent activation. *Nature* **347**, 477-479 (1990).
23. Behrens, C.J., van den Boom, L.P., de Hoz, L., Friedman, A. & Heinemann, U. Induction of sharp wave-ripple complexes in vitro and reorganization of hippocampal networks. *Nat Neurosci* **8**, 1560-1567 (2005).
24. Grover, L.M. Evidence for postsynaptic induction and expression of NMDA receptor independent LTP. *J Neurophysiol* **79**, 1167-1182 (1998).
25. Huang, Y.Y. & Malenka, R.C. Examination of TEA-induced synaptic enhancement in area CA1 of the hippocampus: the role of voltage-dependent Ca2+ channels in the induction of LTP. *J Neurosci* **13**, 568-576 (1993).
26. Brown, T.C., Correia, S.S., Petrok, C.N. & Esteban, J.A. Functional compartmentalization of endosomal trafficking for the synaptic delivery of AMPA receptors during long-term potentiation. *J Neurosci* **27**, 13311-13315 (2007).
27. van Weert, A.W., Geuze, H.J., Groothuis, B. & Stoorvogel, W. Primaquine interferes with membrane recycling from endosomes to the plasma membrane through a direct interaction with endosomes which does not involve neutralisation of endosomal pH nor osmotic swelling of endosomes. *European journal of cell biology* **79**, 394-399 (2000).
28. Mollenhauer, H.H., James Morré, D. & Rowe, L.D. Alteration of intracellular traffic by monensin; mechanism, specificity and relationship to toxicity. *Biochimica et Biophysica Acta (BBA) - Reviews on Biomembranes* **1031**, 225-246 (1990).

29. Sihra, T.S., Flores, G. & Rodriguez-Moreno, A. Kainate Receptors: Multiple Roles in Neuronal Plasticity. *Neuroscientist* (2013).
30. Lynch, G., Larson, J., Kelso, S., Barrionuevo, G. & Schottler, F. Intracellular injections of EGTA block induction of hippocampal long-term potentiation. *Nature* **305**, 719-721 (1983).
31. Malenka, R.C., Kauer, J.A., Zucker, R.S. & Nicoll, R.A. Postsynaptic calcium is sufficient for potentiation of hippocampal synaptic transmission. *Science* **242**, 81-84 (1988).
32. Zong, X. & Lux, H.D. Augmentation of calcium channel currents in response to G protein activation by GTP gamma S in chick sensory neurons. *J Neurosci* **14**, 4847-4853 (1994).
33. Pinheiro, P.S.*, et al.* Selective block of postsynaptic kainate receptors reveals their function at hippocampal mossy fiber synapses. *Cereb Cortex* **23**, 323-331 (2013).
34. Marques, J.M.*, et al.* CRMP2 tethers kainate receptor activity to cytoskeleton dynamics during neuronal maturation. *J Neurosci* **33**, 18298-18310 (2013).
35. Lanore, F.*, et al.* Deficits in morphofunctional maturation of hippocampal mossy fiber synapses in a mouse model of intellectual disability. *J Neurosci* **32**, 17882-17893 (2012).
36. Tashiro, A., Dunaevsky, A., Blazeski, R., Mason, C.A. & Yuste, R. Bidirectional regulation of hippocampal mossy fiber filopodial motility by kainate receptors. A two-step model of synaptogenesis. *Neuron* **38**, 773-784 (2003).
37. Engert, F. & Bonhoeffer, T. Dendritic spine changes associated with hippocampal long-term synaptic plasticity. *Nature* **399**, 66-70 (1999).
38. Matsuzaki, M.*, et al.* Dendritic spine geometry is critical for AMPA receptor expression in hippocampal CA1 pyramidal neurons. *Nat Neurosci* **4**, 1086-1092 (2001).
39. Matsuzaki, M. Factors critical for the plasticity of dendritic spines and memory storage. *Neurosci Res* **57**, 1-9 (2007).
40. Wang, Z.*, et al.* Myosin Vb mobilizes recycling endosomes and AMPA receptors for postsynaptic plasticity. *Cell* **135**, 535-548 (2008).
41. Lerma, J. Kainate receptor physiology. *Current opinion in pharmacology* **6**, 89-97 (2006).
42. Malenka, R.C. & Nicoll, R.A. Long-term potentiation--a decade of progress? *Science* **285**, 1870-1874 (1999).
43. Ylinen, A.*, et al.* Sharp wave-associated high-frequency oscillation (200 Hz) in the intact hippocampus: network and intracellular mechanisms. *J Neurosci* **15**, 30-46 (1995).

44. O'Neill, J., Senior, T. & Csicsvari, J. Place-selective firing of CA1 pyramidal cells during sharp wave/ripple network patterns in exploratory behavior. *Neuron* **49**, 143-155 (2006).
45. Ego-Stengel, V. & Wilson, M.A. Disruption of ripple-associated hippocampal activity during rest impairs spatial learning in the rat. *Hippocampus* **20**, 1-10 (2010).
46. Kato, H.K., Kassai, H., Watabe, A.M., Aiba, A. & Manabe, T. Functional coupling of the metabotropic glutamate receptor, InsP3 receptor and L-type Ca2+ channel in mouse CA1 pyramidal cells. *J Physiol* **590**, 3019-3034 (2012).
47. Miyazaki, K. & Ross, W.N. Ca2+ sparks and puffs are generated and interact in rat hippocampal CA1 pyramidal neuron dendrites. *J Neurosci* **33**, 17777-17788 (2013).
48. Crepel, V. & Mulle, C. Physiopathology of kainate receptors in epilepsy. *Current opinion in pharmacology* **20**, 83-88 (2015).
49. Motazacker, M.M.*, et al.* A defect in the ionotropic glutamate receptor 6 gene (GRIK2) is associated with autosomal recessive mental retardation. *American journal of human genetics* **81**, 792-798 (2007).
50. Petrovic, M.M.*, et al.* Inhibition of post-synaptic Kv7/KCNQ/M channels facilitates long-term potentiation in the hippocampus. *PLoS One* **7**, e30402 (2012).

Figure Legends

Fig 1. **KA increases AMPAR surface expression.**

A, Immunoblots show the KA-evoked increased surface expression of GluA1 and GluA2, which was blocked by CNQX. Data were quantified as % of control, n=3 independent experiments. Dot-plots on the right indicated values for the individual experiments. Unless otherwise indicated, all imaging and biochemistry experiments are performed in the continuous presence of TTX (0.5 µM), GYKI53655 (40 µM) and L689560 (5 µM).

B, Confocal images showing surface GluA1 and GluA2 in the dendritic shaft and spine (scale bar 1 µm) and cumulative frequency plots of spine/dendrite ratios. n=11-16 cells per condition, 3 independent experiments.

C, Co-localization of GluA1 or GluA2 (red) and PSD95 (green). Scale bar 1 µm. Graphs show Pearson´s coefficients for the co-localization. The black line in the whisker plot boxes indicates the median. n=10-15 cells per condition, 3 independent experiments.

D, mEPSCs from CA1 pyramidal cells in hippocampal slices in the continuous presence of APV and ± GYKI and ± KA. Quantification of the data using cumulative distribution plots of mEPSC amplitudes and whisker plots. n=4 cells for control, n=5 cells for KA from n=4 animals.

In all experiments shown in B, C and D, data acquisition and analysis were performed in blind with respect to the treatment.

Fig 2. **KAR activation induces LTP.**

A, Effects of KA on normalized evoked EPSC amplitudes and sample traces from CA1 neurons in the presence of D-APV in mice hippocampal slices. n=5 cells from 5 animals for control and n=6 cells from 6 animals for kainate.

B-C, Schematic representations of the HFS and the RL-LTP induction protocols.

D, Normalized fEPSP slope in WT and GluK2$^{-/-}$ mice subjected to RL-LTP. The symbols for experiments without APV are squares (black for control and white for test pathway), whereas for experiments with APV the symbols are circles (black for control and white for test pathway). Arrow indicates point of RL-LTP stimulation. WT: n=8 slices from 8 animals; WT + AP5: n=9 slices from 3 animals; GluK2$^{-/-}$: n=8 slices from 8 animals; GluK2-/- + AP5 n= 8 slices from 8 animals.

E, Representative traces for D.

F, Normalized fEPSP slope values 21-30 min post LTP protocol.

In all experiments shown in B, C and D, data acquisition and analysis were performed in blind with respect to the treatment or genotype of the animal.

Fig 3. **KAR-LTP induces structural plasticity.**

A, KAR-induced increase in spine size. Right panel shows quantification of spine area after KA (A) / area before KA (A_0) versus time. The period of KA application is indicated by the black bar. n=4-6 cells per condition, 3 independent experiments, Scale bars 1 µm.

B-C, Time-lapse experiments showing KA-induced increase in the number of protrusions and enhanced transition from stubby to mushroom spines. The number of protrusions was quantified before KA application (N_0) and at the indicated times (N) in 10 mm segments of dendrites ± KA. The period of KA application is indicated by the black bar. n=3-6 cells per condition, 3 independent experiments. Scale bars 4 µm.

In all experiments, data analysis was performed in blind with respect to the treatment.

Fig 4. **KAR-LTP recruits rab11-recycling endosomes to spines.**

A, KA (red arrow) recruits transferrin-Alexa594 (red) labelled recycling endosomes to spines. GFP was expressed to visualise morphology. Time is indicated in seconds. Right panel shows the quantification of the proportion of endosomes in head or shaft, n=5-6 cells per condition, 3 independent experiments. Scale bar 1 µm.

B, Dominant negative Rab11 prevents recruitment of recycling endosomes into spines. Tf-A488 positive endosomes (green) in neurons expressing RFP-rab11wt or dn (red). n=6-8 cells per condition, 3 independent experiments. Scale bar 1 µm.

C, Images of spines before (t=0) and 30 min (t=30) after KA +/- CNQX in neurons expressing GFP, Rab11wt or Rab11dn. Frequency distribution plots of individual spine diameters before (black, t=0) and after (grey dotted line, t=30 min) KA. n=4-5 cells per condition, 3 independent experiments. Scale bar 1 µm.

In all experiments, data analysis was performed in blind with respect to the treatment.

Fig 5. **KAR-LTP requires intracellular calcium increase, PKC and PLC activation.**

A-B, BAPTA-AM, U73122 and chelerythrine, but not EDTA, block KAR-mediated increase in co-localization of surface GluA1 or GluA2 (red) and PSD95 (green). Scale bar 1 µm. Box-

and-whisker plots show range of Pearson´s coefficient of controls (see also Supplementary Fig. 5) and KA treated cells (KA). Black line in the boxes indicates the median. n=6-15 cells per condition, 3 independent experiments. Data analysis was performed in blind with respect to the pharmacological treatment.

C, Images of spines before (t=0) and 30 min (t=30) after indicated drugs +/- KA. Corresponding graphs on the right show frequency distribution of individual spine diameters before (black, t=0) and after (grey dotted line, t=30 min) KA. n=4 cells per condition, 3 independent experiments. Note that extracellular chelation of calcium by EDTA does not prevent KAR-mediated increase in structural plasticity. Data analysis was performed in blind with respect to the pharmacological treatment.

D-E, Effects of KA on normalized evoked EPSC amplitudes and sample traces from CA1 neurons in the presence of chelerythrine (upper panel) or the PLC inhibitor U-73122 (bottom panel) in mice hippocampal slices. n=6 slices from 2 animals for chelerythrine and n=7 slices from 2 animals for U-73122.

F, Box-and-whisker plots show range of fold increase in PLC (right) and PKC (left) activity after KA challenge. PLC or PKC activity was normalized to controls in the presence of the indicated drugs. Black line in the boxes indicates the median. n=4-6 independent experiments.

Fig 6. **KAR-LTP requires KAR metabotropic signalling.**

A, Box-and-whisker plots show range of fold increase in PLC (right) and PKC (left) in cells preincubated with PTX. PLC or PKC activity was normalized to control and performed in parallel with the experiment in figure 5C. Black line in the boxes indicates the median. n=4-6 independent experiments.

B, Co-localization of surface GluA1 or GluA2 (red) and PSD95 (green). Scale bar 1 µm. Box-and-whisker plots of Pearson´s coefficients of colocalization indicate that the metabotropic pathway inhibitor PTX blocks KAR-evoked increase in surface AMPARs. Black line in the boxes indicates the median. n=9-13 cells per condition, 3 independent experiments.

C, PTX blocks KAR-mediated increase in CA1 mEPSC amplitude (compare to Fig. 1D). n=3 cells from 3 animals. Examples of traces pretreated with PTX before and after GYKI53655 (control) and shown before and after KA plus GYKI53655 (KA+GYKI). Graphs show cumulative frequency distribution of mEPSC amplitudes and box-and-whisker plots in insets indicating range.

D, Preincubation with PTX impaired the KA-induced increase of normalized evoked EPSC amplitudes in WT mice hippocampal slices (compare with Fig. 2A). Sample traces are shown before and after KA challenge. n=6 cells from 3 animals per condition.

E, Normalized fEPSP slope recorded in WT-mice hippocampal slices pretreated with PTX. Arrow indicates point of LTP induction. n=7 slices from 4 animals.

F, Images of spines before (t=0) and 30 min (t=30) after KA in cells treated with PTX. Frequency distribution of individual spine diameters before (black, t=0) and after (red, t=30 min) KA. n=3 cells per condition, 3 independent experiments.

In all experiments data analysis was performed in blind with respect to the treatment.

Fig 7. **KAR-LTP does not require ionotropic KAR activation.**

A, Box-and-whisker plots show fold increase in PLC (right) and PKC activity (left) in the presence of the ionotropic KAR inhibitor UBP310 (10 µM). PLC or PKC activity was normalized to control and performed in parallel with the experiments in figure 5C. Black line in the boxes indicates the median. n=6 independent experiments.

B, UBP310 (10 µM) did not impair the KA-induced increase of normalized evoked EPSC amplitudes in WT mice hippocampal slices (compare with Fig. 2A). Sample traces are shown before and after KA challenge. n=5 cells from 4 animals.

C, Normalized fEPSP slope recorded in WT mice hippocampal slices in the presence of UBP310 (10 µM). Arrow indicates time point of LTP induction. n=11 slices per condition from 6 animals.

D, Images of spines before (t=0) and 30 min (t=30) after KA in cells treated UBP310 (10 µM). Frequency distribution of individual spine diameters before (black, t=0) and after (red, t=30 min) KA. n=4-6 cells per condition, 3 independent experiments. Data analysis was performed in blind with respect to the pharmacological treatment.

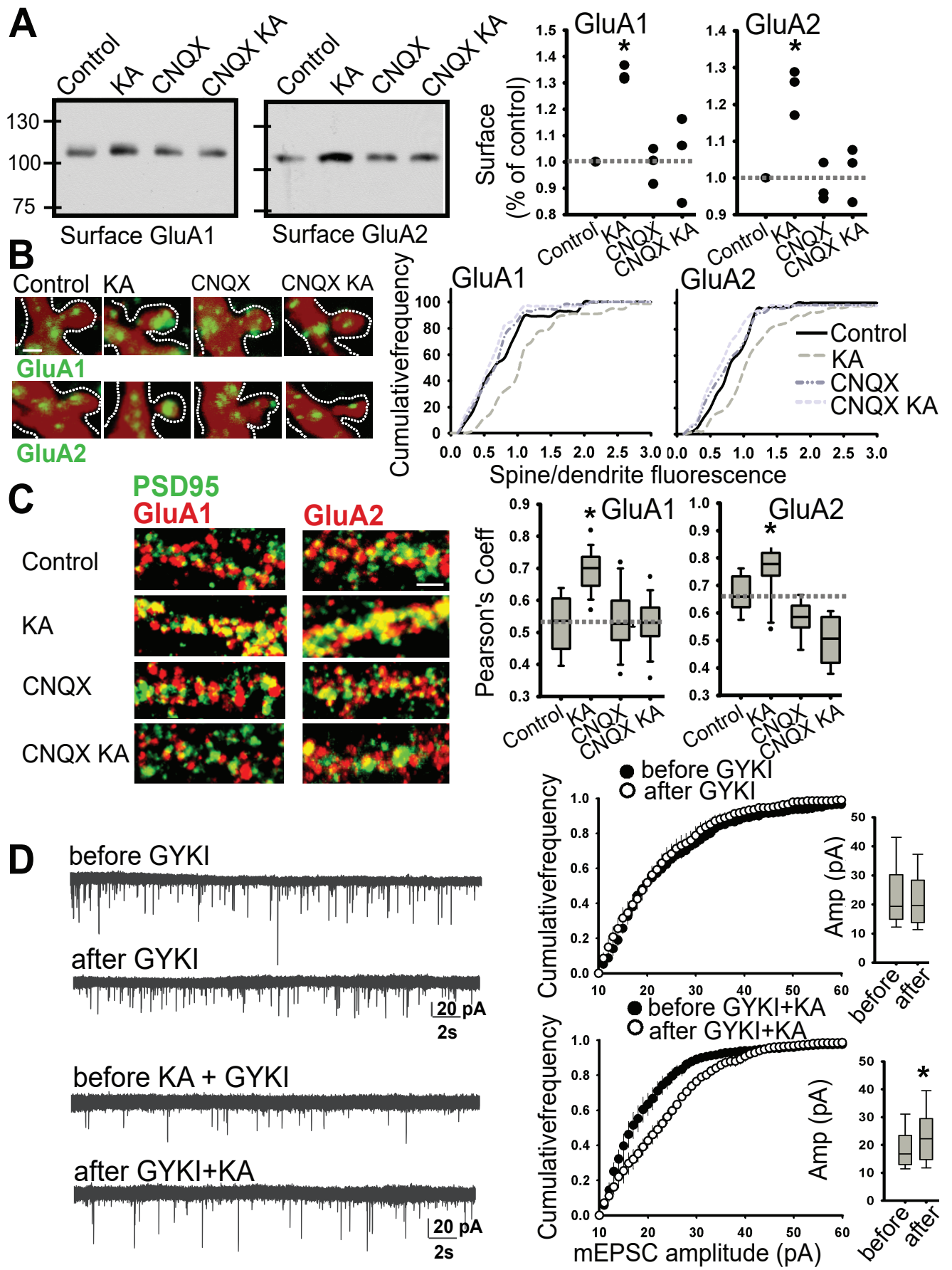
A
Control
KA
CNQX
CNQX KA
130
100
75
Surface GluA1
Surface GluA2
GluA1
GluA2
Surface (% of control)
B
Control
KA
CNQX
CNQX KA
GluA1
GluA2
Cumulativefrequency
Spine/dendrite fluorescence
C
PSD95
GluA1
GluA2
Control
KA
CNQX
CNQX KA
Pearson's Coeff
D
before GYKI
after GYKI
20 pA
2s
before KA + GYKI
after GYKI+KA
before GYKI+KA
after GYKI+KA
Amp (pA)
before
after
mEPSC amplitude (pA)

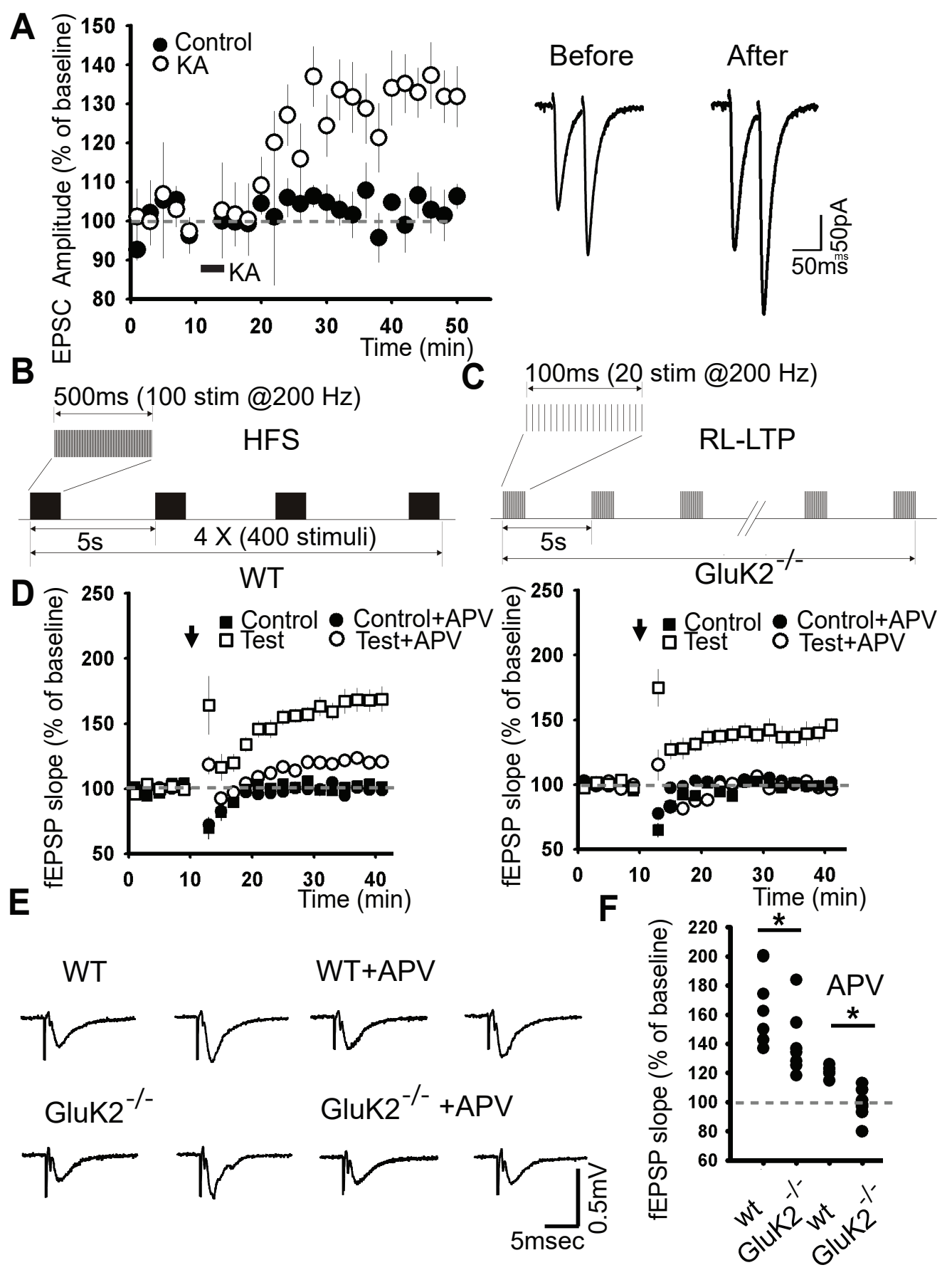
A
Control
KA
KA
EPSC Amplitude (% of baseline)
Time (min)
Before
After
50pA
50ms
B
500ms (100 stim @200 Hz)
HFS
5s
4 X (400 stimuli)
C
100ms (20 stim @200 Hz)
RL-LTP
5s
WT
GluK2-/-
D
Control
Control+APV
Test
Test+APV
fEPSP slope (% of baseline)
Time (min)
E
WT
WT+APV
GluK2-/-
GluK2-/- +APV
0.5mV
5msec
F
fEPSP slope (% of baseline)
APV
wt
GluK2-/-
wt
GluK2-/-

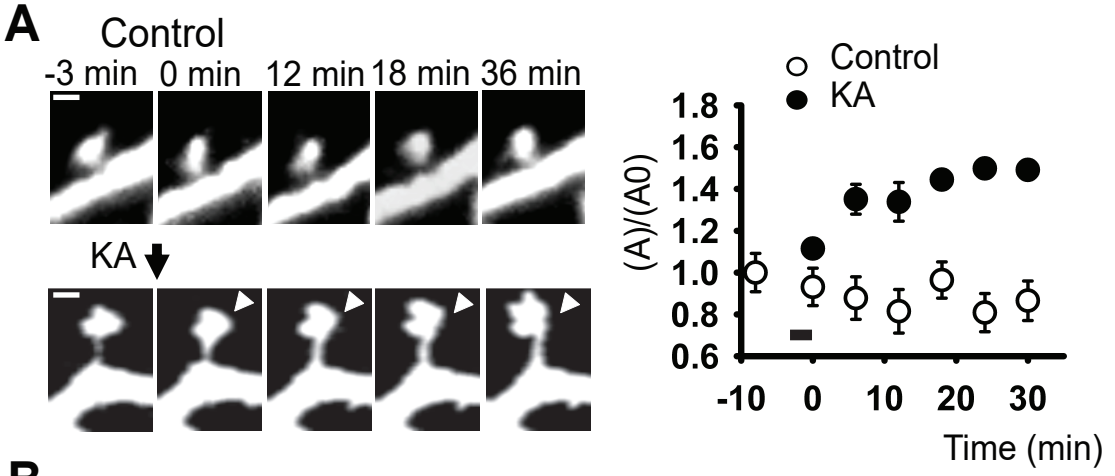

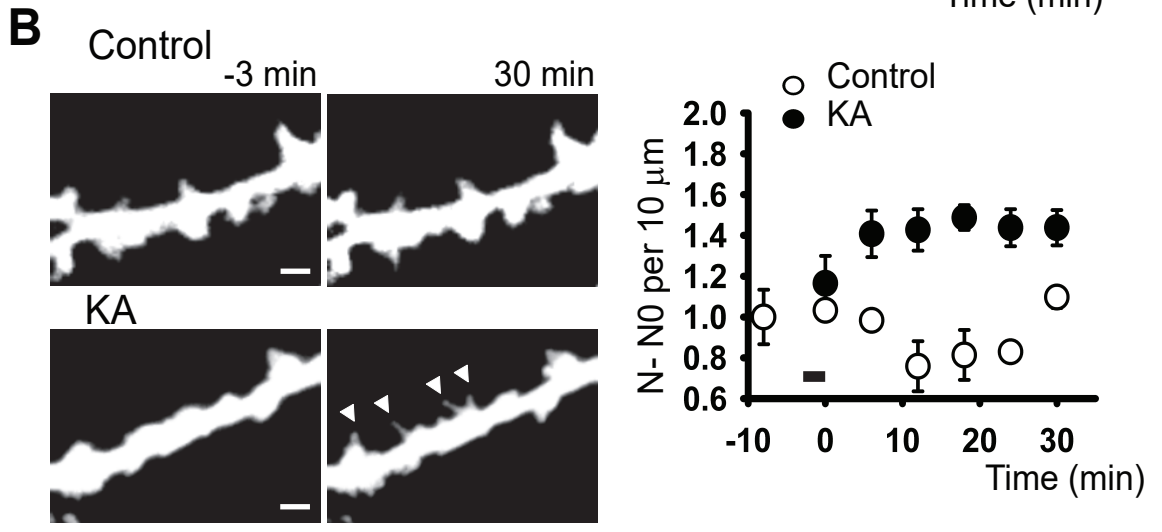

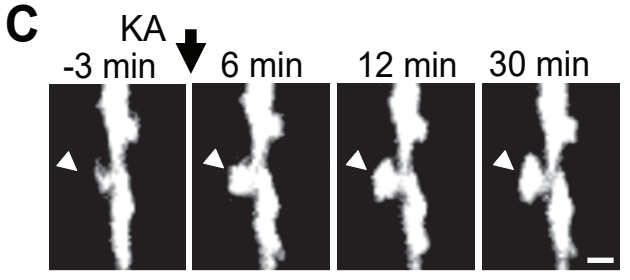

	% Stubby to Mushroom
Control	-13.95±3
KA	18.75±4

*

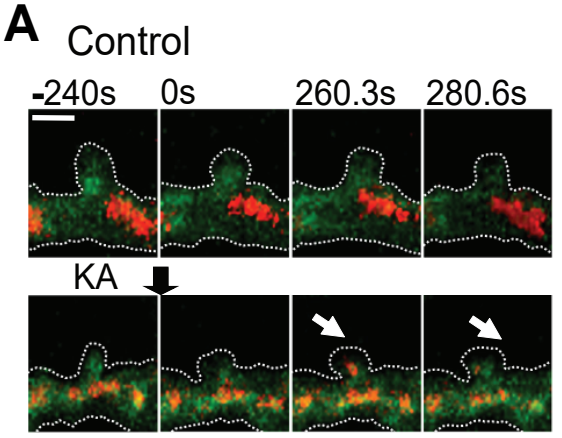

	% of spines containing Tf-A594	
	Head Ω	Shaft Ω
Control	12.6±7	68.5±1.5
KA	51.6±7.8	16.6±0.3

*

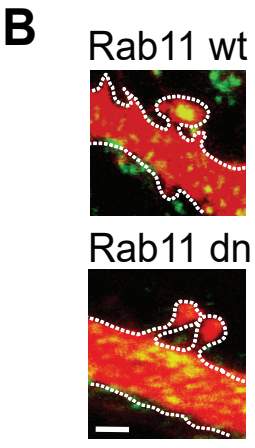

	% of spines containing Tf-A594	
	Head Ω	Shaft Ω
Rab11 wt KA	59.7±7	18.0±2
Rab11 dn KA	20.0±3.3	65.5±6.5

*

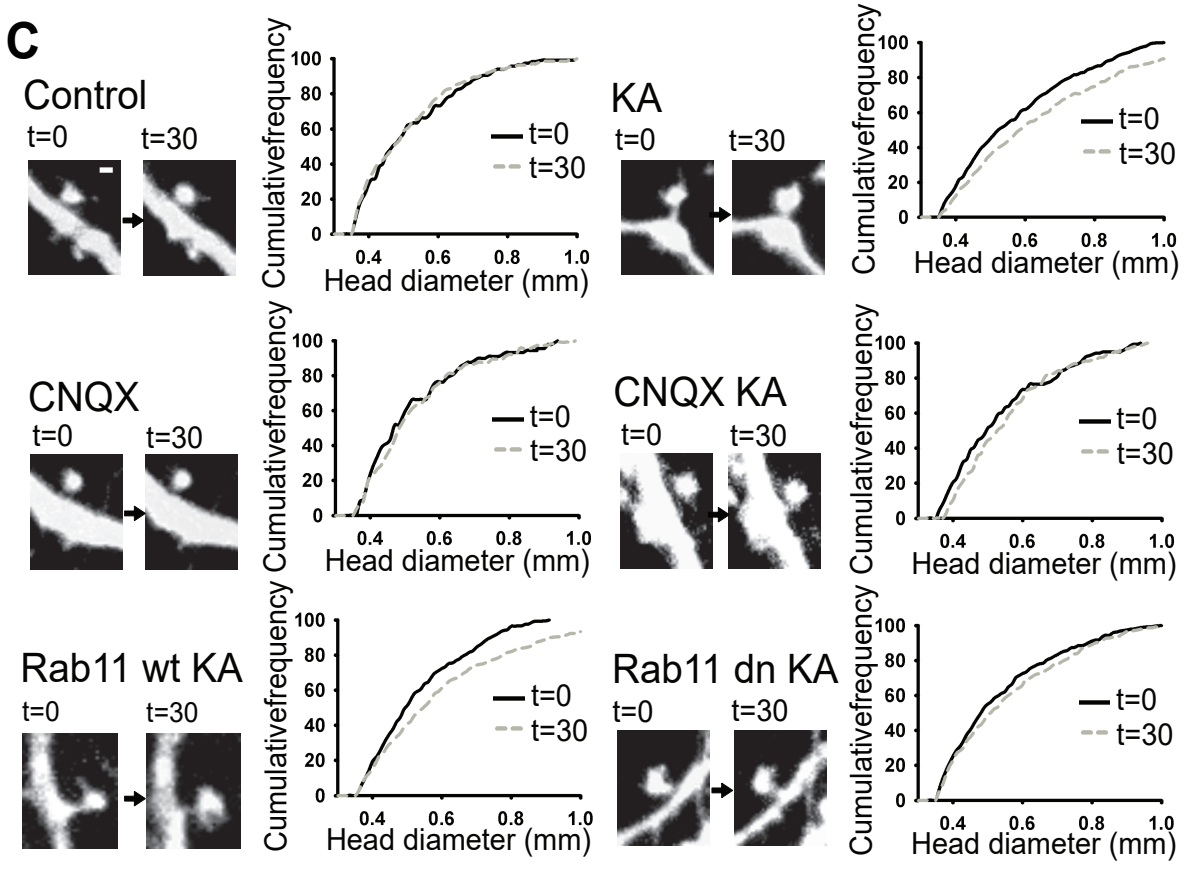

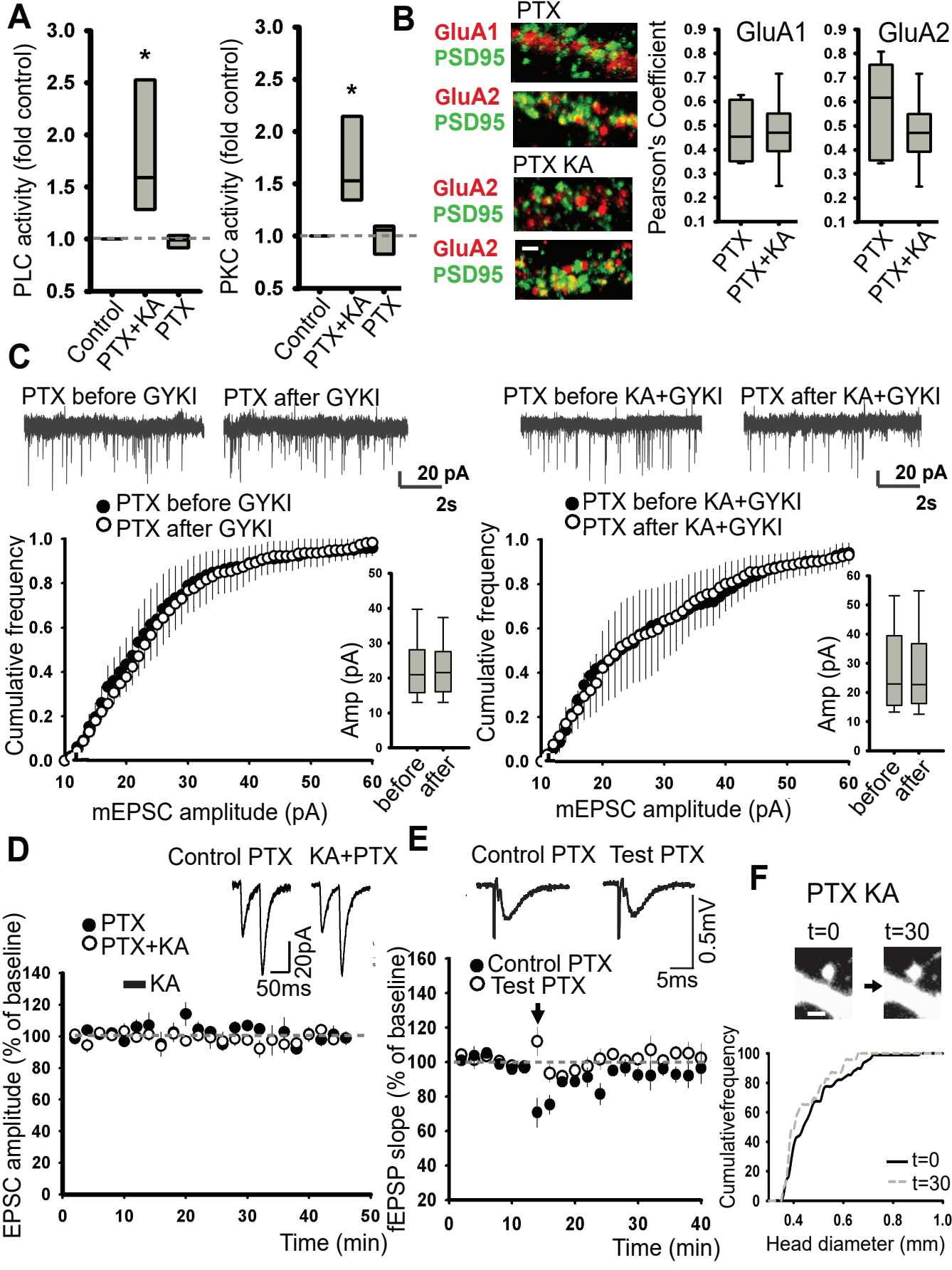
A
PLC activity (fold control)
PKC activity (fold control)
Control
PTX+KA
PTX
B
PTX
GluA1
PSD95
GluA2
PSD95
PTX KA
GluA2
PSD95
GluA2
PSD95
Pearson's Coefficient
GluA1
GluA2
PTX
PTX+KA
C
PTX before GYKI
PTX after GYKI
PTX before KA+GYKI
PTX after KA+GYKI
20 pA
2s
Cumulative frequency
mEPSC amplitude (pA)
Amp (pA)
before
after
D
Control PTX
KA+PTX
PTX
PTX+KA
KA
50ms
20pA
EPSC amplitude (% of baseline)
Time (min)
E
Control PTX
Test PTX
0.5mV
5ms
fEPSP slope (% of baseline)
Time (min)
F
PTX KA
t=0
t=30
Cumulativefrequency
Head diameter (mm)

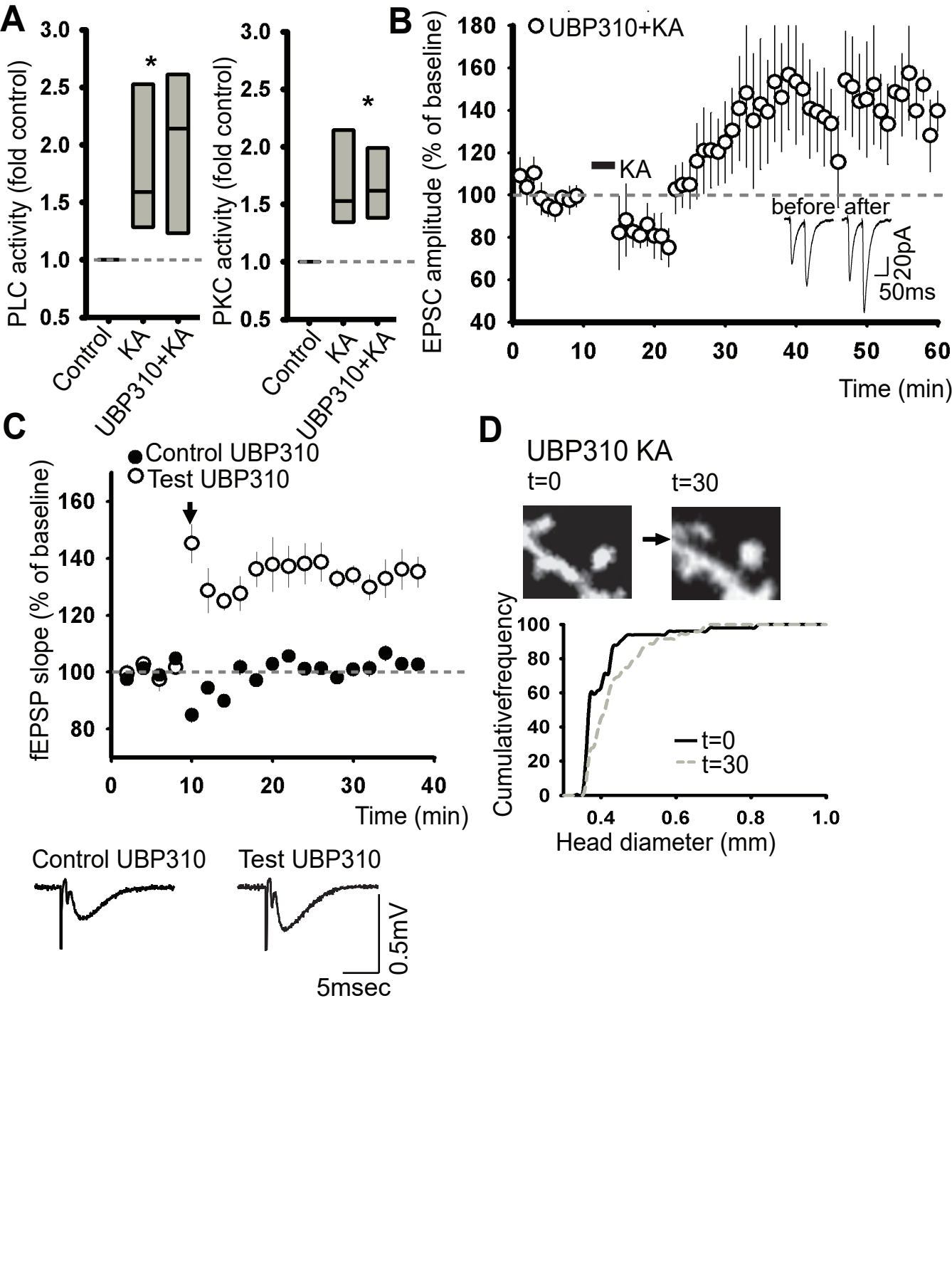
A
PLC activity (fold control)
PKC activity (fold control)
3.0
2.5
2.0
1.5
1.0
0.5
*
Control
KA
UBP310+KA
B
EPSC amplitude (% of baseline)
UBP310+KA
KA
before after
20pA
50ms
180
160
140
120
100
80
60
40
0
10
20
30
40
50
60
Time (min)
C
Control UBP310
Test UBP310
fEPSP slope (% of baseline)
160
140
120
100
80
0
10
20
30
40
Time (min)
Control UBP310
Test UBP310
0.5mV
5msec
D
UBP310 KA
t=0
t=30
Cumulativefrequency
100
80
60
40
20
0
t=0
t=30
0.4
0.6
0.8
1.0
Head diameter (mm)

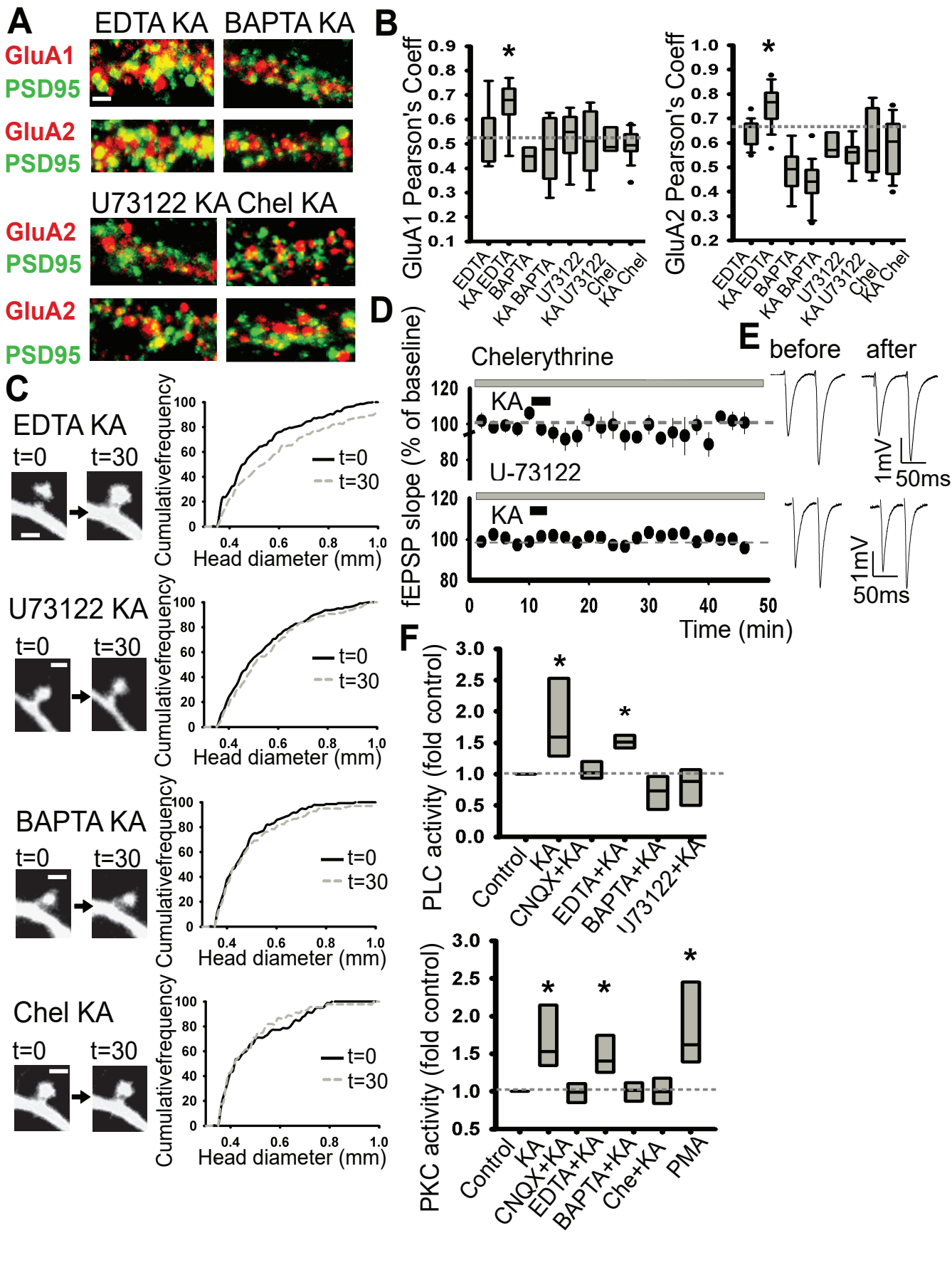
A
EDTA KA
BAPTA KA
GluA1
PSD95
GluA2
PSD95
U73122 KA
Chel KA
GluA2
PSD95
GluA2
PSD95
B
GluA1 Pearson's Coeff
GluA2 Pearson's Coeff
EDTA
KA EDTA
BAPTA
KA BAPTA
U73122
KA U73122
Chel
KA Chel
C
EDTA KA
t=0
t=30
U73122 KA
BAPTA KA
Chel KA
Cumulativefrequency
Head diameter (mm)
D
Chelerythrine
KA
U-73122
fEPSP slope (% of baseline)
Time (min)
E
before
after
1mV
50ms
F
PLC activity (fold control)
Control
KA
CNQX+KA
EDTA+KA
BAPTA+KA
U73122+KA
PKC activity (fold control)
Che+KA
PMA